Peer-reviewed version available at *J. Mar. Sci. Eng.* **2018**, *6*, 50; doi:10.3390/jmse6020050

Article

Experimental investigation of propeller wake velocity field for the major factors affecting propeller wake wash

Md. Asif Amin[a,*], Bruce Colbourne[a], Brian Veitch[a]

[a] Memorial University of Newfoundland, Faculty of Engineering and Applied Science, 40 Arctic Ave, St. John's, NL A1B 3X7, Canada. Email: maa633@mun.ca; bruce.colbourne@mun.ca; bveitch@mun.ca

* Correspondence: maa633@mun.ca

Abstract: The propeller jet from a ship has a significant component directed upwards towards the free surface of the water, which can be used for ice management. This paper describes a comprehensive laboratory experiment where the influences of operational factors affecting a propeller wake velocity field were investigated. The experiment was done on a steady wake field to investigate the characteristics of the axial velocity of the fluid in the wake and the corresponding variability downstream of the propeller. The axial velocities and the variability recorded were time-averaged. Propeller rotational speed was found to be the most significant factor, followed by propeller inclination. The experimental results also provide some idea about the change of the patterns of the mean axial velocity distribution against the factors considered for the test throughout the effective wake field, as well as the relationships to predict the axial velocity for known factors.

Keywords: ship's propeller jet; mean axial velocity of flow; prediction equations

1 Introduction

Propeller wake wash can be used as a means of clearing pack ice and small ice masses from the vicinity of offshore installations and shipping channels. In a full-scale study of various pack ice management techniques performed offshore Newfoundland, propeller wake wash was found to be the only mechanism to have an appreciable degree of success [2]. In more recent studies of ice management techniques, the wake of an azimuth thruster was shown to be useful for ice breaking [12, 13], in addition to clearing ice from designated areas. Propeller wake wash was found to be an effective means of breaking ice ridges, and pushing away medium sized ice floes and even glacial ice. This technique enables ice management without having any physical interaction with ice.

The interaction between an ice mass and a propeller jet depends on the jet velocity at a particular location downstream of propeller, which depends on propeller shaft rotational speed (n), propeller inclination (θ), and propeller submergence from the fluid surface (H). The application of propeller wake wash as an ice management tool has been investigated at model tank scale by Ferrieri [8], where change in ice concentration was investigated as a function of the factors affecting propeller wake wash. Bastin [3] developed a simple mathematical model of propeller wake wash based on Ferrieri's experimental results.

Preprints (www.preprints.org) | NOT PEER-REVIEWED | Posted: 1 April 2018 doi:10.20944/preprints201804.0004.v1

Peer-reviewed version available at J. Mar. Sci. Eng. 2018, 6, 50; doi:10.3390/jmse6020050

Brewster [6] reported that a propeller jet velocity decays exponentially as it moves downstream from the propeller plane, or efflux plane. Lam et al. [14, 15] reported that the tangential velocity is already significantly diminished a distance $x/D_p = 3.68$ downstream from the propeller. McGarvey [16] and Brewster [6] reported that the radial velocity decays by about 80% within $x/D_p = 0.30$ from the efflux plane. In the present study, only the axial component of fluid velocity is considered, which is expected to be significant throughout the wake field, and important for ice management.

Nomenclature (all S.I. units)

C_t	Thrust coefficient of the propeller	V_0	Efflux velocity
d	Vertical distance from the water surface	V_{Axial}	Axial velocity in the wake
D_p	Propeller diameter	$V_{MaxAxial}$	Maximum axial velocity
D_h	Propeller hub diameter	x	Longitudinal distance from efflux plane
H	The depth of submergence of propeller	y	Distance from the center of the wake
n	Propeller rotational speed	Z	Number of propeller blades
R_p	Propeller radius	β	Propeller blade area ration
Re_{flow}	Flow Reynolds number	σ	Standard deviation (variability of flow)
Re_{prop}	Propeller Reynolds number	ν	Viscosity of fluid ($kg.m^2s^{-1}$)

2 Methodology

The experiment was designed using the center composite design (CCD) technique of response surface methodology for three factors (propeller- rotational speed, inclination and submergence) tested at five levels. A total of 18 combinations of the three factors was considered, and measurements were taken at 168 locations in the wake field, thereby requiring 3,024 measurements for each response variable. The length of the wake field covered in the experiment was $x/D_p = 30.5$, which was divided into three zones: near field ($x/D_p \leq 3.5$), intermediate field ($3.5 \leq x/D_p \leq 15.5$) and far field ($15.5 \leq x/D_p \leq 30.5$). The response variable of interest was the mean axial flow velocity.

2.1 Design of Experiment

The required minimum number of factorial combinations for the experimental design was calculated as = $\{2^3 + (2x3) + 1\} = 15$. Three extra center point runs (combinations of factors) were added to the experiment to ensure an accurate estimation of experimental error [17]. Design Expert 10.0 software [7] was used to obtain the combinations of factors and to analyze the results. The values of factors used at five levels during the experiment are listed in Table 1.

Table 1. Factors used at different levels of the experiment

Factors	Low axial	Low	Centre	High	High axial
Shaft rotational speed (rps)	6.0	7.0	9.0	11.0	12.0
Propeller inclination (deg.)	0.0	1.5	4.5	7.5	9.0
Submergence of propeller (mm)	200	250	350	450	500

Preprints (www.preprints.org) | NOT PEER-REVIEWED | Posted: 1 April 2018 doi:10.20944/preprints201804.0004.v1

Peer-reviewed version available at J. Mar. Sci. Eng. 2018, 6, 50; doi:10.3390/jmse6020050

The lowest propeller rotational speed was 6.0 rps, which was determined on the basis of the formula for Reynolds numbers (Propeller Reynolds number 'Re_{prop}', and Flow Reynolds number 'Re_{flow}') to meet the requirement for minimum Reynolds number, such that the viscous scaling effect on the experimental results can be neglected [19].

2.2 Experimental Set-up

The experiment was done in a tow tank (Length x Breadth x Depth = 58.27 x 4.57 x 3.04 meter). The arrangement of equipment used in the experiment is shown in Fig. 1. The major components were the open boat propulsion unit, the EMCM (Electro-magnetic Current Meter) sensors, and the data acquisition system.

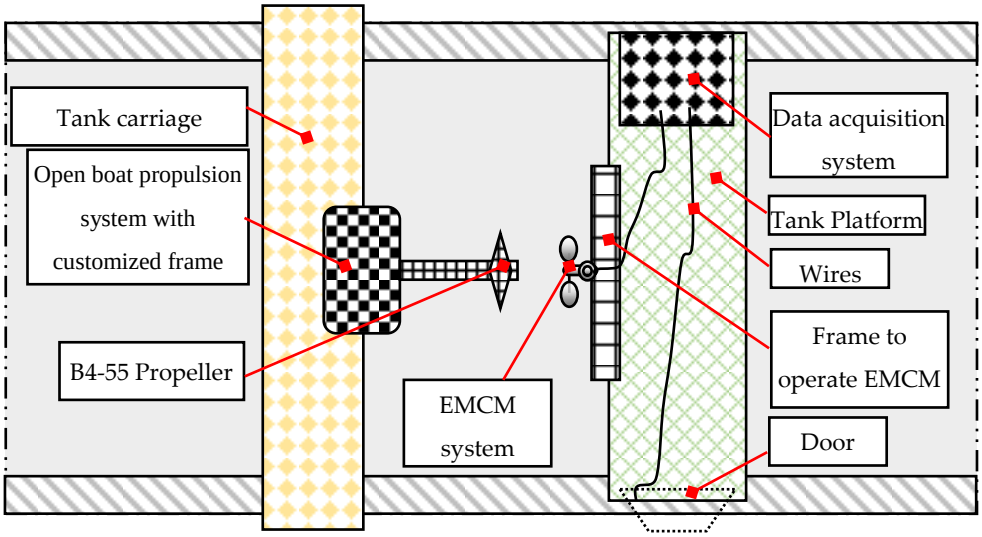

Fig. 1: Schematic of experimental set-up

A B-series propeller of diameter 250 mm was located at the center of the tank. The wake survey was carried out under the bollard pull condition. A stock open boat propulsion unit was used to drive the propeller.

2.3 Scaling Effect

The variables of the prediction model were non-dimensionalized using 'Buckingham-π theory'. The viscous scaling effects of the experimental results were checked using the empirical formula developed by Verhey [19], who suggested that the scaling effect due to viscosity is negligible, if the Reynolds number of the propeller (Re_{prop}) and the Reynolds number of the flow (Re_{flow}) are greater than $7x10^4$ and $3x10^3$ respectively, for a propeller wake. Verhey used the formulae: $Re_{flow} = \frac{V_0 D_P}{\nu}$ and $Re_{prop} = \frac{nL_m D_P}{\nu}$, where V_0 = efflux velocity of the propeller jet, and $V_0 = 1.59 n D_P \sqrt{C_t}$ [9], C_t is the thrust coefficient of model propeller, D_P = Propeller diameter, n = propeller rotational speed (rps), ν = kinematic viscosity of fluid (water) = 1.0023E-6 m^2/s at 20°C; L_m = length term dependent on blade area ratio (β), number of blades of propeller (N), diameter of hub (D_h) and D_P. L_m is defined (Blaauw and van de Kaa, 1978) as: $L_m = \beta . D_p . \pi . \left\{2N\left(1 - \frac{D_h}{D_p}\right)\right\}^{-1}$. According to Verhey's formulas, the

Preprints (www.preprints.org) | NOT PEER-REVIEWED | Posted: 1 April 2018 doi:10.20944/preprints201804.0004.v1

Peer-reviewed version available at J. Mar. Sci. Eng. 2018, 6, 50; doi:10.3390/jmse6020050

Reynolds numbers for the lowest shaft rotational speed (6 rps) of the model propeller were Re_{flow} = 2.87x10^5 and Re_{prop} = 8.54 x10^4.

2.4 Open Boat Propulsion System

The open boat propulsion system integrates all the equipment that was used to generate the propeller wake under a particular propulsion condition. A total of 18 experimental conditions were used to develop the prediction models. The unit consisted of the propeller, the open boat propulsion unit, and the frame to locate the open boat unit on the carriage of the tow tank. The propeller was a B4-55 series of diameter Ø = 250 mm. The frame had a mechanism of adjusting the inclination of the propeller. The power delivered was adjustable which was synchronized to the shaft rotational speed of propeller. Table 2 illustrates the properties of the prototype propeller.

Table 2. Properties of model propeller

Diameter, D_p	250 mm	Bollard thrust coeff., C_t	0.306
Hub diameter, D_h	42 mm	Bollard torque coeff., C_q	0.041
Blade Arear Ratio, β	55	Number of blades, N	4

2.5 EMCM Equipment

An EMCM (Electro-magnetic Current Meter) system was used to measure the wake flow velocity during the experiment. This system included an EMCM package (EMCM sensors and a built-in mounting to maintain the orientation of sensors) to measure the axial flow velocity, a frame to mount and operate the sensors, a linear displacement transducer to measure the transverse displacement of the sensors, a platform to support the system equipment, and connecting wires. The tank platform was installed across the breadth of the tank (4.57 meter), on the top of which the EMCM equipment with the supporting frame, and the data acquisition system were installed. The EMCM sensors could slide on the frame with respect to a datum. The datum was marked at the center of the wake field (y = 0). The readings along the transverse direction of the propeller wake (along y/D_P) were collected by sliding the sensors following a pre-marked scale on the frame. The EMCM system was connected with the data acquisition system, where all the data were recorded and stored immediately after the capture of the reading. In the experiment, each measurement was taken for a period of at least 30s at 4Hz.

3 Results and Discussion

The objective of this study was to determine the influence of the three input factors (Table 1) affecting the propeller wake wash. A total of 18 propeller conditions (experimental runs) comprising different combinations of the three factors were used to create an experimental plan with the Design Expert 10.0 software for a Centre Composite Design (CCD) of the Response Surface Methodology. The resulting data were used to develop prediction equations for the mean axial velocity of flow in the wake. Flow velocity measurements were taken longitudinally and transversely covering half-width of the wake field for three water depths (d = 0.25D_P, 0.55D_P and 1.05D_P). A decision was made to assume longitudinal symmetry about the mid plane and thus only to survey the half width of wake field based on empirical analyses performed by earlier researchers

Preprints (www.preprints.org) | NOT PEER-REVIEWED | Posted: 1 April 2018 doi:10.20944/preprints201804.0004.v1

Peer-reviewed version available at J. Mar. Sci. Eng. 2018, 6, 50; doi:10.3390/jmse6020050

[4, 5, 6, 10, 11, 14, 16, 18, 19]. These all reported the axisymmetric nature of the wake velocity distribution for the far zone downstream of propeller wake. This allowed a more detailed survey of the flow within the limitations of time and resources.

3.1 Individual Effect of Factors

Initially the influences of individual factors on the mean axial velocity of flow were assessed by applying an analysis approach known as 'One Factor at a Time (OFAT)'. In OFAT, the configurations of factors were selected such that only one factor was varied at a time, keeping the other two factors unchanged. Three cases were considered illustrating the individual effect of each factor. The combinations of factors in each case are shown in Table 3 (below).

Table 3. Combinations of factors under each case to assess the individual effect of factors

Case #1: Influence of propeller rotational speed 'n' on the mean axial velocity of flow			
Selected Runs	'n' in rps	'θ' in degree	'H' in mm
Run #1	6	4.5	350
*Centre Point Run	9	4.5	350
Run #16	12	4.5	350
Case #2: Influence of propeller inclination angle 'θ' on the mean axial velocity of flow			
Selected Runs	'n' in rps	'θ' in degree	'H' in mm
Run #5	9	0.0	350
*Centre Point Run	9	4.5	350
Run #2	9	9.0	350
Case #3: Influence of propeller depth of submergence 'H' on the mean axial velocity of flow			
Selected Runs	'n' in rps	'θ' in degree	'H' in mm
Run #14	9	4.5	200
*Centre Point Run	9	4.5	350
Run #13	9	4.5	500

*Values for Centre Point Run are the average of the four centre point runs (combinations of factors) considered in the experiment (n = 9 rps, θ = 4.5°, H = 350 mm)

The above cases illustrate the effect of each factor on the mean axial flow velocity along the normalized dimension x/D_P (longitudinally downstream of propeller). The transverse location for this data was along the center of the wake field ($y/D_P = 0$), where the tank wall boundary effect was the minimum.

3.1.1 Individual effect of factors on mean axial flow velocity

Case #1: The individual effect of propeller shaft rotational speed (n) on the mean axial velocity of flow (V_a) along x/D_P at the center of the wake field ($y/D_P = 0$) is illustrated in Figures 2a ~ 2c for the three different depths of measurements: $0.25D_P$, $0.55D_P$ and $1.05D_P$ respectively. These illustrate that the mean axial velocity along the centerline generally increases with 'n'.

Preprints (www.preprints.org) | NOT PEER-REVIEWED | Posted: 1 April 2018 doi:10.20944/preprints201804.0004.v1

Peer-reviewed version available at J. Mar. Sci. Eng. 2018, 6, 50; doi:10.3390/jmse6020050

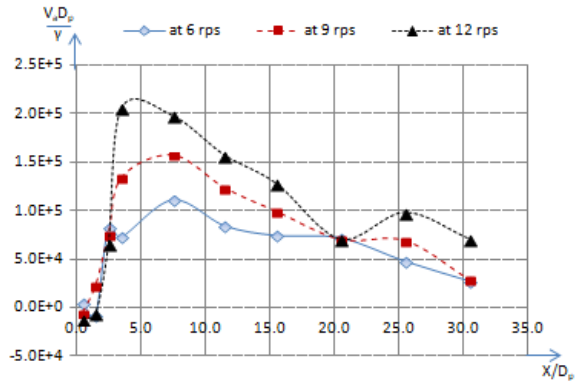

Fig. 2a

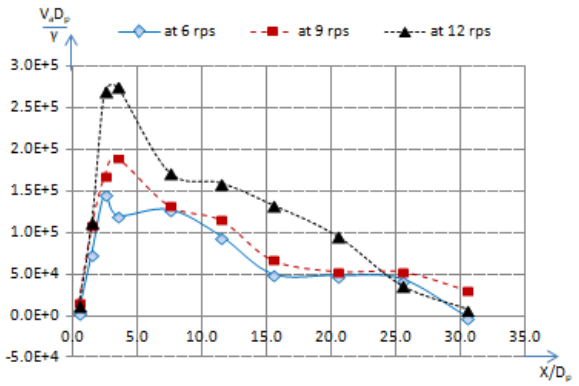

Fig. 2b

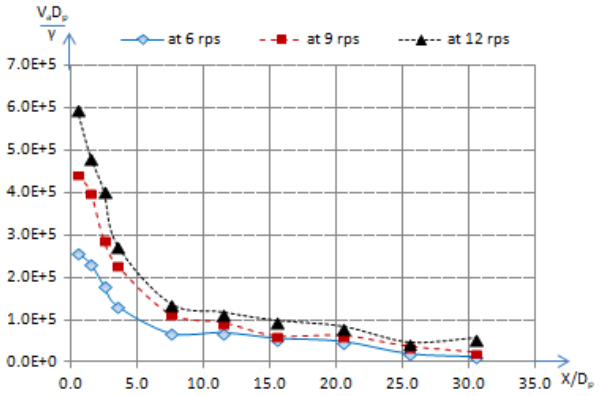

Fig. 2c

Case #2: The individual effect of propeller inclination (θ) on the mean axial velocity of flow (V_a) along x/D_P at the center of the wake field ($y/D_P = 0$) is illustrated in Figures 3a ~ 3c for the three depths of measurements: $0.25D_P$, $0.55D_P$ and $1.05D_P$ respectively. These illustrate that the characteristics of the mean axial velocity along x/D_P with 'θ' depend on the depth. In general at shallow depth the mean axial velocity increases with 'θ', and the effect of 'θ' reduces with increasing depth.

The effect of propeller inclination on the mean axial velocity is most pronounced near the surface and negligible at the lowest depth. Moreover the effect of 'θ' is also not as strong as 'n'. This phenomenon becomes clearer in 3D surface plots in the following section.

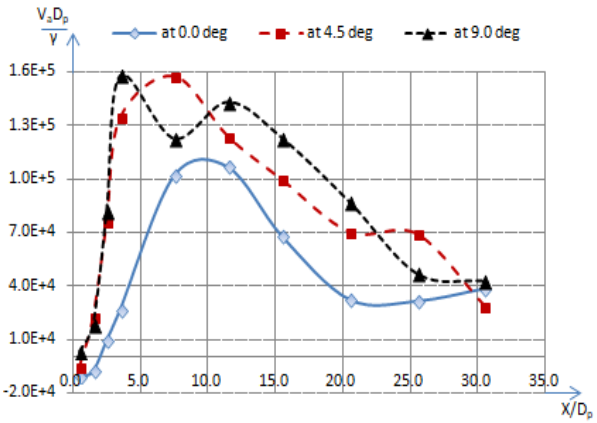

Fig. 3a

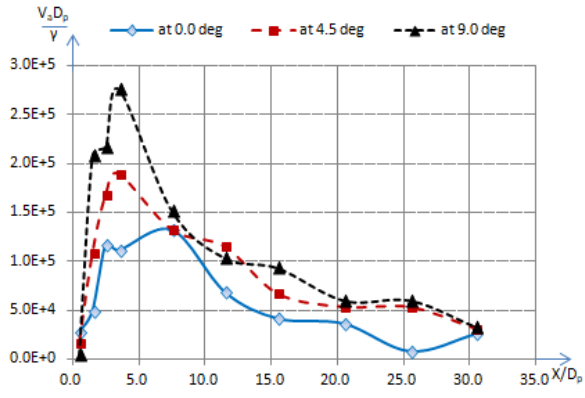

Fig. 3b

Preprints (www.preprints.org) | NOT PEER-REVIEWED | Posted: 1 April 2018 doi:10.20944/preprints201804.0004.v1

Peer-reviewed version available at J. Mar. Sci. Eng. 2018, 6, 50; doi:10.3390/jmse6020050

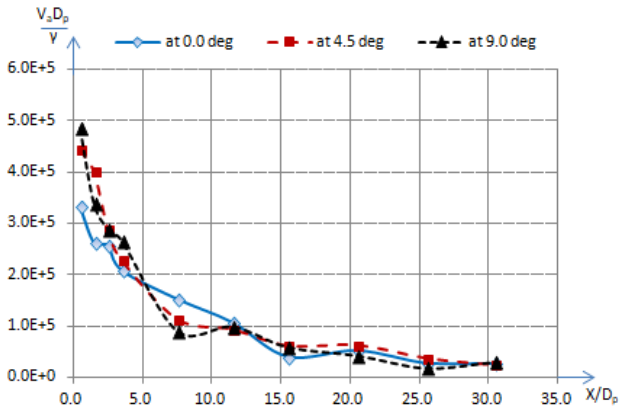

Fig. 3c

Case #3: The individual effect of propeller submergence (H) on the mean axial flow velocity (V_a) along x/D_P at the center of the wake field ($y/D_P = 0$) are illustrated in Figures 4a ~ 4c for the three different depths of measurements: $0.25D_P$, $0.55D_P$ and $1.05D_P$ respectively. These plots illustrate that the characteristics of the mean axial velocity along x/D_P with 'H' also largely depend on the depth. In general, at shallow depth the axial velocity increases with decreasing 'H', and at deeper depth the mean axial velocity is not significantly affected in the downstream and shows mixed effects in the region near the propeller.

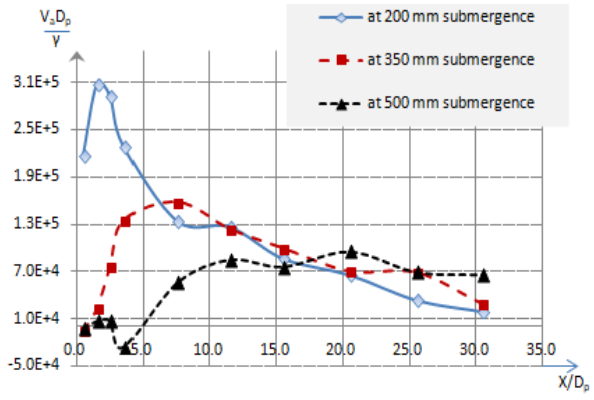

Fig. 4a

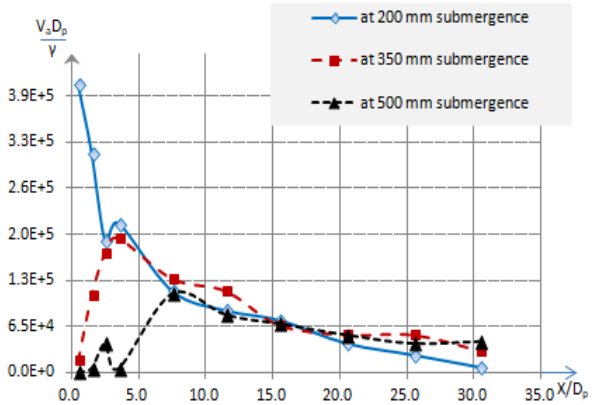

Fig. 4b

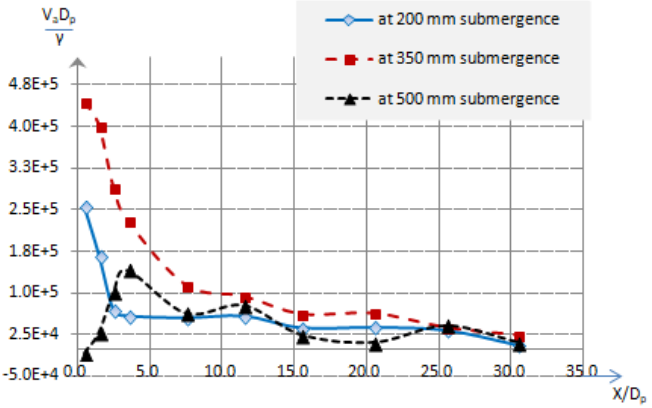

Fig. 4c

Preprints (www.preprints.org) | NOT PEER-REVIEWED | Posted: 1 April 2018 doi:10.20944/preprints201804.0004.v1

Peer-reviewed version available at J. Mar. Sci. Eng. 2018, 6, 50; doi:10.3390/jmse6020050

3.1.2 Individual effect of factors on the mean axial velocity of flow along y/D_P at $0.25D_P$

Given that the focus of this study is on the use of wake flow in ice management, the wake flow at the surface is more significant in terms of effect on floating ice. Thus the surface flow characteristics were analyzed in more detail.

Case #1: The individual effect of propeller shaft rotational speed (n) on the non-dimensionalized mean axial velocity of flow $\left(\frac{V_a D_P}{\nu}\right)$ along y/D_P at various longitudinal locations (x/D_P) are illustrated in Figure 5, for the depth of measurement closest to the water surface, which was d = $0.25D_P$. The two longitudinal locations closest to the propeller (at x/D_P = 0.50 and 1.50) are ignored due to the confused flow in those regions. The readings taken at the locations close to the tank wall were affected by the boundary condition, so are ignored for developing the curves within the plots (Fig. 5-7). Therefore, the curves illustrating the distribution of the mean axial velocities along y/D_P are the approximate pattern of the velocity distribution along y/D_P.

Figure 5 illustrates that the mean axial velocity along y/D_P also increases with 'n'. Also the mean axial velocity along transverse locations is the highest at x/D_P = 7.50 for all three 'n' considered in the study, where θ = 4.5° and H = 350 mm.

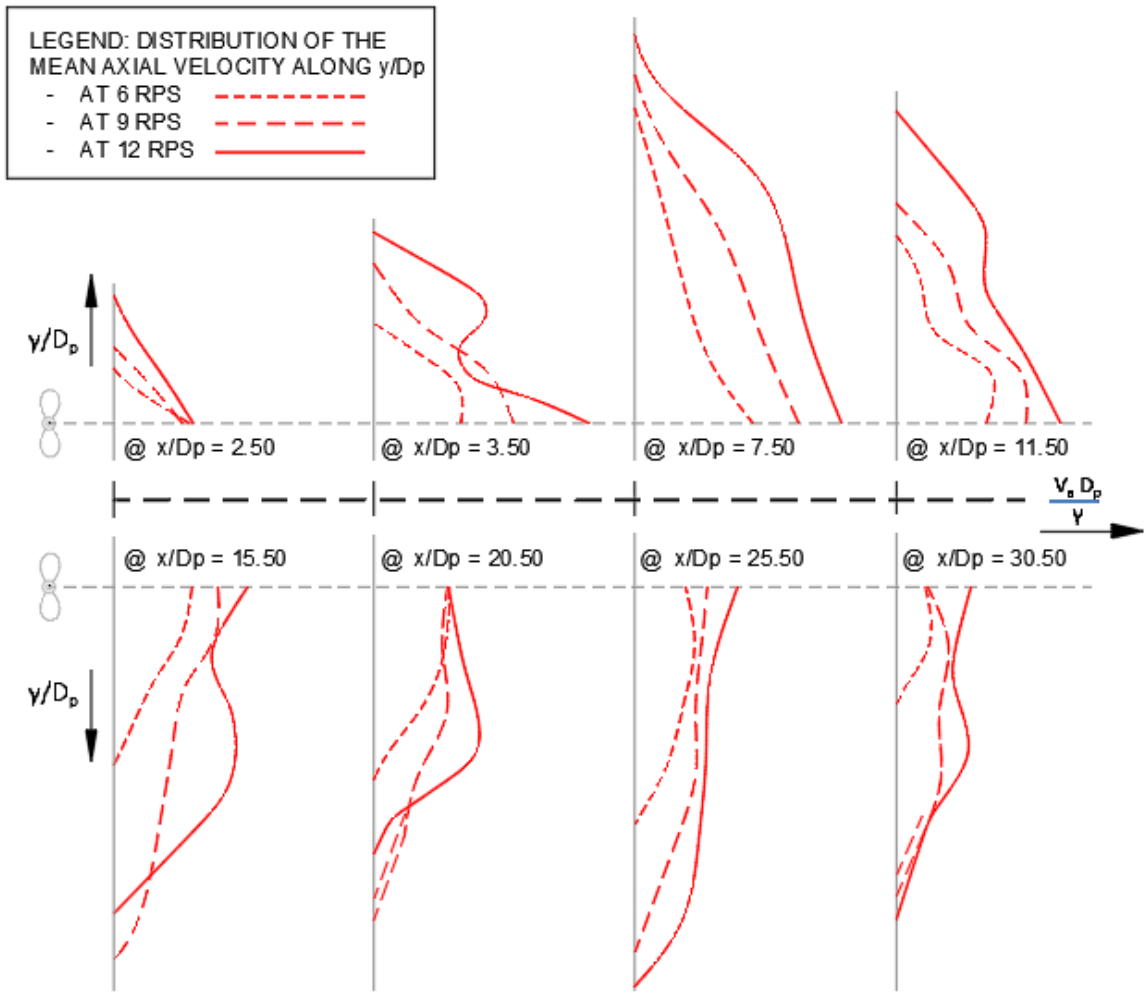

Fig. 5: showing the approximate patterns of the distribution of the non-dimensionalized mean axial velocities $\left(\frac{V_a D_P}{\nu}\right)$ along y/D_P with the change of 'n'

Preprints (www.preprints.org) | NOT PEER-REVIEWED | Posted: 1 April 2018 doi:10.20944/preprints201804.0004.v1

Peer-reviewed version available at J. Mar. Sci. Eng. 2018, 6, 50; doi:10.3390/jmse6020050

Case #2: The individual effect of propeller inclination (θ) on the mean axial velocity of flow (V_a) along y/D_P at various longitudinal locations (x/D_P) is illustrated in Fig. 6, for the depth closest to the water surface. Fig. 6 shows that, the mean axial velocity along y/D_P generally increases with 'θ', but the changes are different at different locations. Also the changes are not as significant as those due to 'n'. The locations of the highest velocities also depend on 'θ'. At θ = 0°, the most effective zone (the overall mean axial velocities in the zone are higher than other zones) is approximately at x/D_P = 11.50. At θ = 4.5°, the most effective zone is approximately at x/D_P = 7.50. At θ = 9°, the most effective zone is approximately from x/D_P = 11.5 to 15.5.

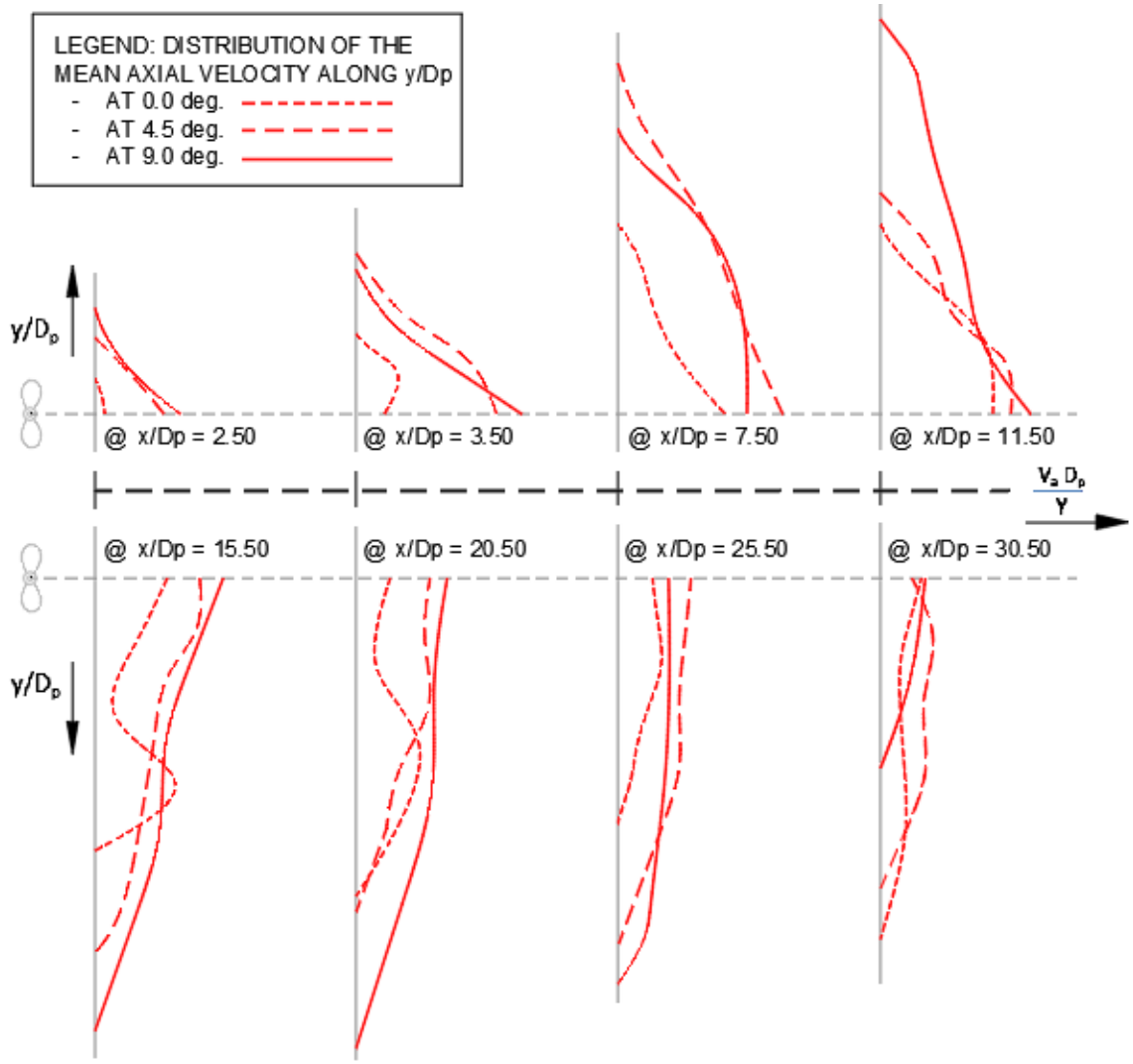

Fig. 6: showing the approximate patterns of the distribution of the non-dimensionalized mean axial velocities $\left(\frac{V_a D_P}{\nu}\right)$ along y/D_P with the change of 'θ'

Preprints (www.preprints.org) | NOT PEER-REVIEWED | Posted: 1 April 2018 doi:10.20944/preprints201804.0004.v1

Peer-reviewed version available at J. Mar. Sci. Eng. 2018, 6, 50; doi:10.3390/jmse6020050

Case #3: The individual effect of propeller submergence (H) on the mean axial velocity (V_a) along y/D_p at various longitudinal locations (x/D_p) is illustrated in Fig. 7, for the depth of measurement closest to the water surface. The effect of 'H' on the mean axial velocity is opposite to the other factors, particularly at the near field ($x/D_p \leq 3.5$) and intermediate field ($3.5 \leq x/D_p \leq 15.5$) zones. With a decrease of 'H' the mean axial velocity increases at any location in the near field and the intermediate field zones, whereas the effect of 'H' is inconsistent in the far field zone.

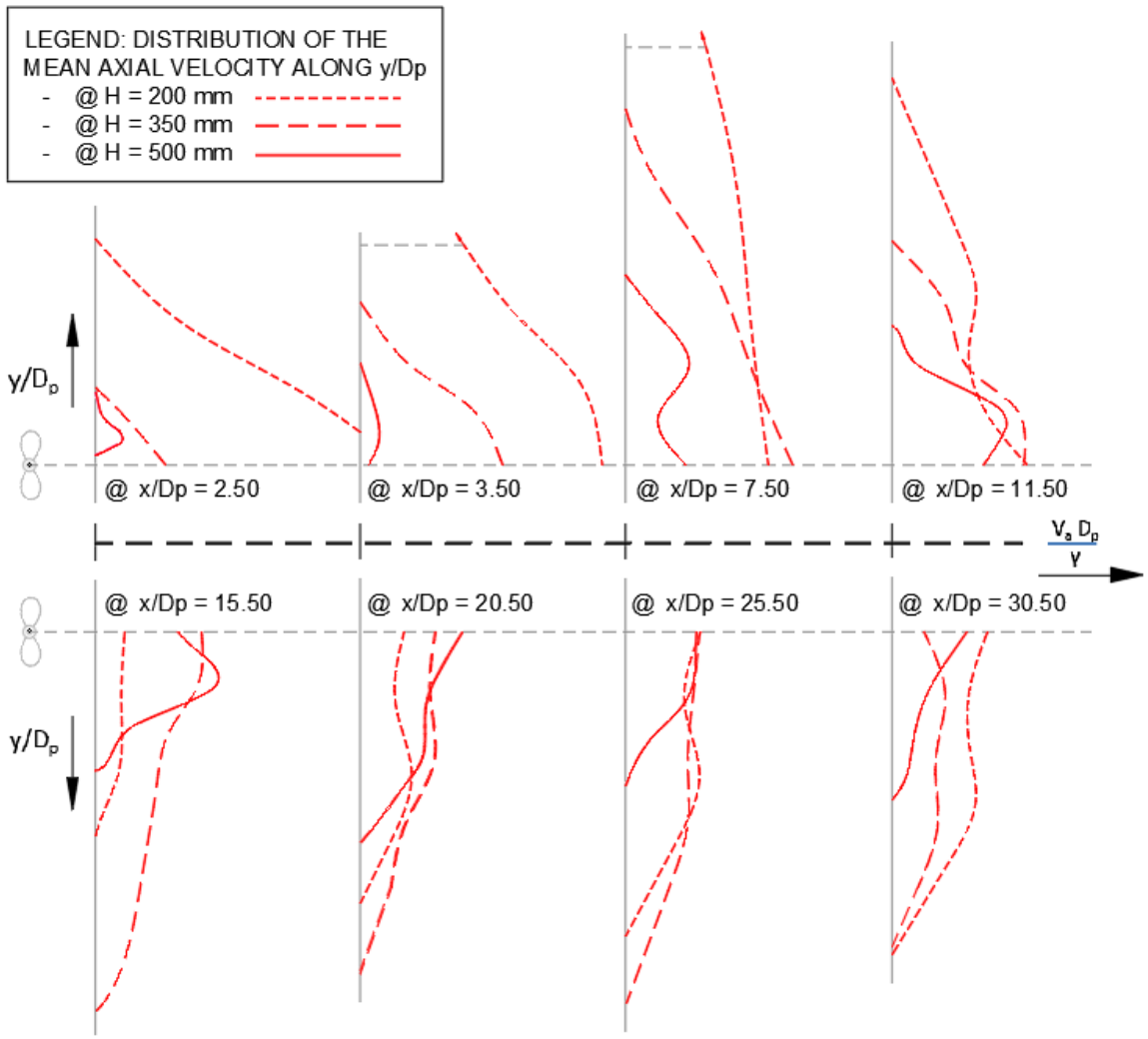

Fig. 7 showing the approximate patterns of the distribution of the non-dimensionalized mean axial velocities $\left(\frac{V_a D_p}{\nu}\right)$ along y/D_p with the change of 'H'

The effects of each of the three factors on the response variable are illustrated explicitly from the study. But the interaction effect of the factors can be shown through a 3D plot or a regression equation.

Preprints (www.preprints.org) | NOT PEER-REVIEWED | Posted: 1 April 2018 doi:10.20944/preprints201804.0004.v1

Peer-reviewed version available at J. Mar. Sci. Eng. 2018, 6, 50; doi:10.3390/jmse6020050

3.2 Interaction Effect of Factors

The interaction effect of multiple factors can be represented by regression equations or 3D contour / surface plots, which show the relationship between factors and the effect on the response variable for each location. In this section, 3D surface plots showing the two-factorial-interaction (2FI) effect of the most influential factors (filtered by the Design Expert software) are presented for locations along the center of the wake field at the depth of measurement closest to the fluid surface ($d = 0.25D_P$). The locations that are selected for the investigation are at $x/D_P = 7.5$, 11.5 and 15.5 at $d = 0.25D_P$, where the overall mean axial velocity was higher than other zones. Additional plots are provided in [1], which is the basis of this paper. Figures 8a ~ 8c) show the change of the non-dimensionalized mean axial velocity with the change of both 'n' and 'θ' along the center of the wake field at $x/D_P = 7.5$, 11.5 and 15.5 at $d = 0.25D_P$ respectively.

These plots show that, at $x/D_P = 7.5$ the velocity increases with 'n' and 'θ', but the effect of 'n' is larger than 'θ'. The effect of 'θ' gradually diminishes and the effect of 'n' decreases with x/D_P. Also it is noticeable that, the effect of 'n' in comparison to the effect of 'θ' is greater at all three locations, and it is expected that this trend will be applicable for all locations downstream in the wake field.

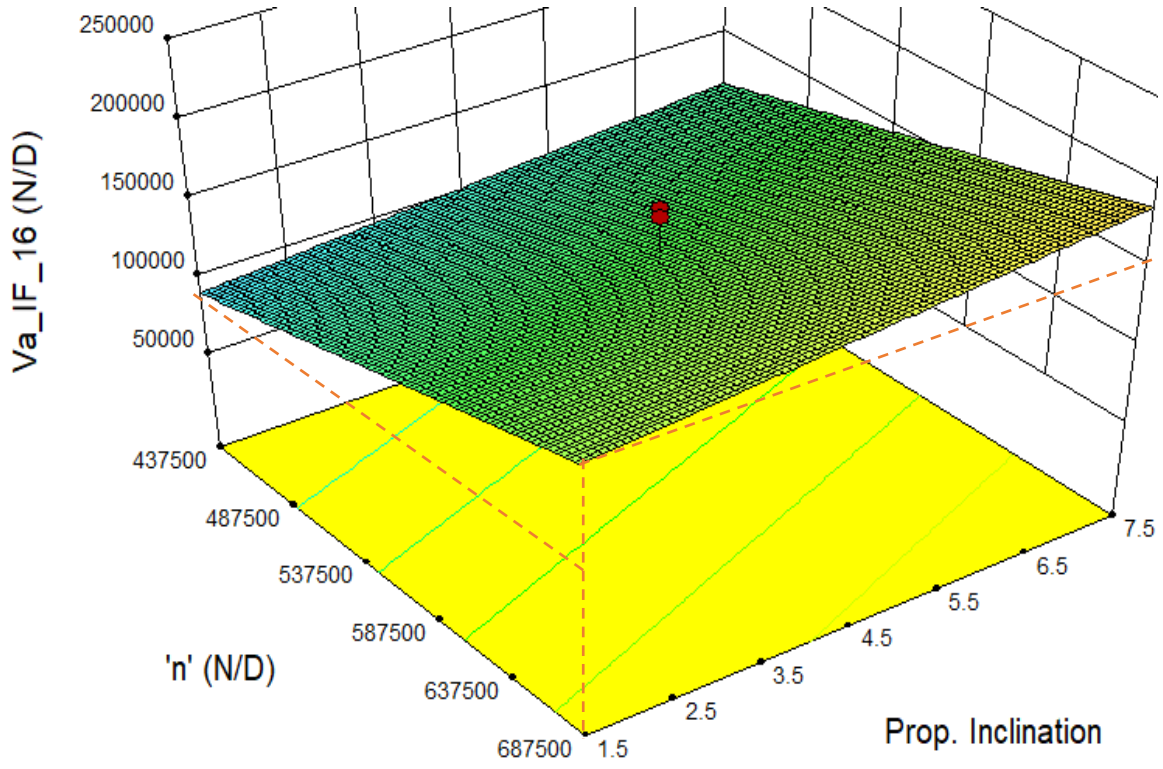

Fig. 8a

Preprints (www.preprints.org) | NOT PEER-REVIEWED | Posted: 1 April 2018 doi:10.20944/preprints201804.0004.v1

Peer-reviewed version available at J. Mar. Sci. Eng. 2018, 6, 50; doi:10.3390/jmse6020050

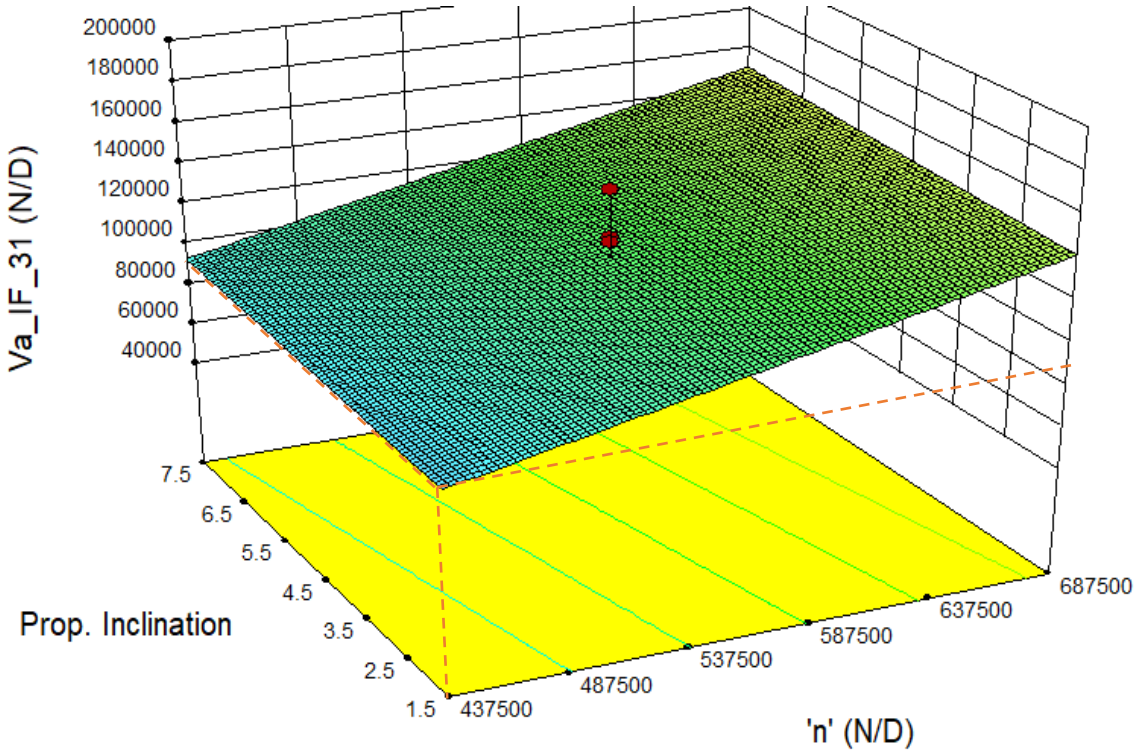

Fig. 8b

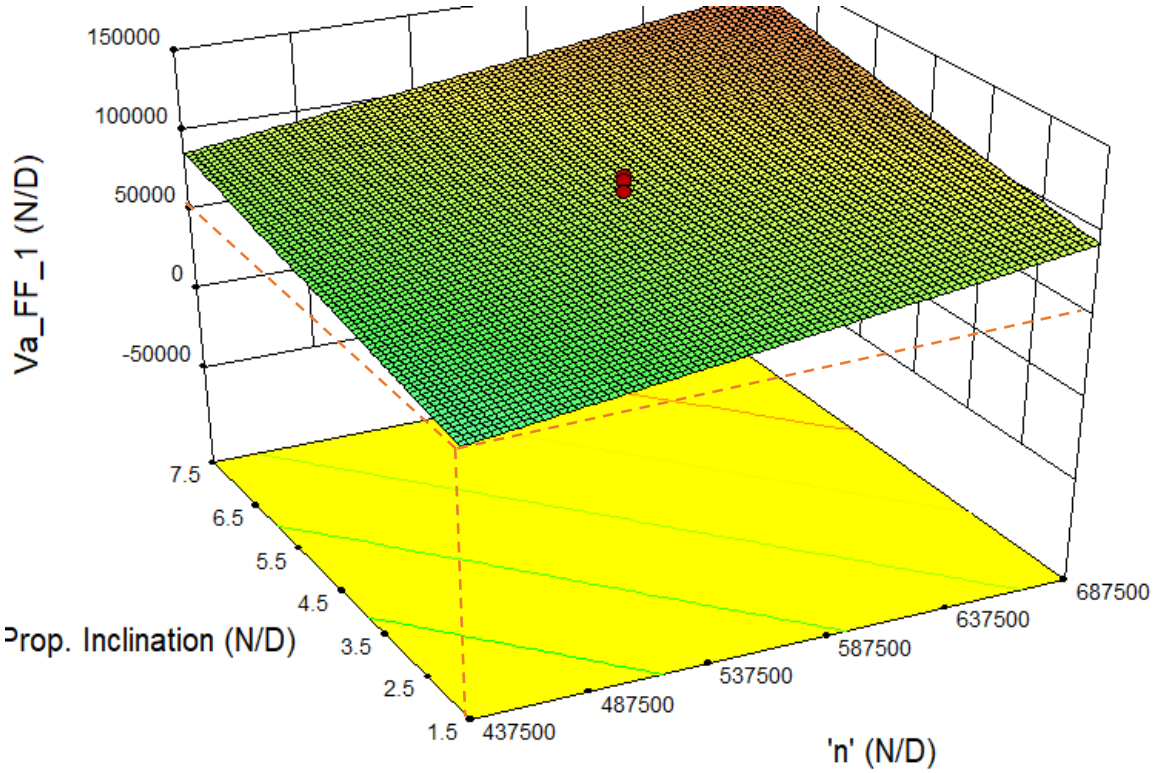

Fig. 8c

Preprints (www.preprints.org) | NOT PEER-REVIEWED | Posted: 1 April 2018 doi:10.20944/preprints201804.0004.v1

Peer-reviewed version available at J. Mar. Sci. Eng. 2018, 6, 50; doi:10.3390/jmse6020050

3.3 Axial Velocity Prediction Equations

The functional relationship between the non-dimensionalized response variable (non-dimensionalized by mean axial velocity) and the non-dimensionalized input factors can be expressed as follows:

$$\frac{V_a D_p}{\nu} = f\left(\frac{nD_p^2}{\nu}, \theta, \frac{H}{D_p}\right)$$

The Buckingham-π theory was used to develop the non-dimensionalized functional relationship among the factors: propeller rotational speed 'n', inclination of propeller 'θ', depth of submergence of propeller 'H', and the response variable of the study, which is mean axial velocity of fluid 'V_a'.

Assuming: $\frac{V_a D_p}{\nu} = V_A$, $\frac{nD_p^2}{\nu} = X$, $\theta = Y$, and $\frac{H}{D_p} = Z$; the common form of the quadratic equation representing the relationship among the factors and the mean axial velocity can be written as:

$$V_A = K + aX + bY + cZ + a_1XY + b_1XZ + c_1YZ + a_2X^2 + b_2Y^2 + c_2Z^2 \quad \ldots\ldots (A)$$

There are ten unknown coefficients in the relationship among the factors and the response, values which depend on the location $\left(\frac{x}{D_p}, \frac{y}{D_p}, \frac{d}{D_p}\right)$ of measurement. Relationships between $\frac{x}{D_p}$, $\frac{y}{D_p}$, $\frac{d}{D_p}$ and the corresponding coefficients were also developed for each zone (near field, intermediate field and far field), which are shown in Tables 4.1-4.3. The kinematic viscosity of water (ν) is considered as 1.0023E-6 m^2/s to calculate the coefficients.

Table 4.1. Regression equations for predicting K, a, b, c, a_1, b_1, c_1, a_2, b_2 and c_2 for Near Field zone

Coeff. of (A) 'K' – 'c_2'	Prediction Equations of the unknown coefficients (K ~ c_2) for **Near Field** zone, obtained through stepwise regression analysis incorporating up to cubic terms
K	K = 479548 – {258367*(y/D_P)} – {1075757*(d/D_P)*(d/D_P)*(d/D_P)} + {1399716*(d/D_P)*(d/D_P)*(y/D_P)} – {561931*(d/D_P)*(y/D_P)*(y/D_P)}
a	a = 0.369 – {0.052*(x/D_P)} + {0.0336*(y/D_P)} – {0.030*(d/D_P)}
b	b = 34935 + {19327*(x/D_P)} – {121413*(d/D_P)} – {28062*(y/D_P)} – {5435*(x/D_P)*(x/D_P)} + {85102*(d/D_P)*(y/D_P)}
c	c = - 520828 + {343649*(y/D_P)*(y/D_P)} + {1656413*(d/D_P)*(d/D_P)*(d/D_P)} – {1321759*(d/D_P)*(d/D_P)*(y/D_P)}
a_1	Ignored, as this coefficient is too small (average = 5.70E-03) to affect the field
b_1	b_1 = - 0.069 – {0.344*(x/D_P)} – {0.470*(d/D_P)} + {0.574*(y/D_P)} + {0.0515*(x/D_P)*(x/D_P)} – {0.245*(y/D_P)*(y/D_P)} + {0.379*(x/D_P)*(d/D_P)} + {0.0367*(x/D_P)*(y/D_P)} + {0.191*(d/D_P)*(y/D_P)} – {0.190*(x/D_P)*(d/D_P)*(y/D_P)}
c_1	c_1 = - 10949 + {3232*(x/D_P)} + {44920*(d/D_P)*(y/D_P)} + {57454*(d/D_P)*(d/D_P)*(d/D_P)} – {82479*(d/D_P)*(d/D_P)*(y/D_P)}
a_2	Ignored, as this coefficient is too small (average = 9.69E-09) to affect the field
b_2	b_2 = 0.369 – {0.052*(x/D_P)} + {0.0336*(y/D_P)} – {0.03033*(d/D_P)}
c_2	c_2 = 223033 – {790287*(d/D_P)*(y/D_P)} – {705383*(d/D_P)*(d/D_P)*(d/D_P)} + {1155228*(d/Dp)*(d/Dp)*(y/Dp)}

Preprints (www.preprints.org) | NOT PEER-REVIEWED | Posted: 1 April 2018 doi:10.20944/preprints201804.0004.v1

Peer-reviewed version available at J. Mar. Sci. Eng. 2018, 6, 50; doi:10.3390/jmse6020050

Table 4.2. Regression equations for predicting K, a, b, c, a_1, b_1, c_1, a_2, b_2 and c_2 for Intermediate Field zone

Coeff. of (A) 'K' – 'c_2'	Prediction Equations of the unknown coefficients (K ~ c_2) for **Intermediate Field**, obtained through stepwise regression analysis incorporating up to cubic terms
K	$K = 53956 - \{456792*(y/D_P)\} + \{278313*(y/D_P)*(y/D_P)\} - \{40801*(y/D_P)*(y/D_P)*(y/D_P)\}$
a	$a = 0.3135 - \{0.0055*(x/D_P)\} - \{0.288*(y/D_P)\} - \{0.0243*(d/D_P)\}$
b	$b = -7788 + \{4985*(y/D_P)\}$
c	$c = 143033 + \{229377*(y/D_P)\} - \{194465*(y/D_P)*(y/D_P)\} + \{30873*(y/D_P)*(y/D_P)*(y/D_P)\}$
a_1	$a_1 = 0.011 - \{0.007*(y/D_P)\}$
b_1	$b_1 = -0.154 + \{0.356*(d/D_P)\} - \{0.092*(y/D_P)\} + \{0.0335*(y/D_P)*(y/D_P)\} - \{0.084*(d/D_P)*(y/D_P)\}$
c_1	$c_1 = 22893 - \{1396*(x/D_P)\} - \{7321*(y/D_P)\} + \{481*(x/D_P)*(y/D_P)\}$
a_2	Ignored, as this coefficient is too small (average = 9.61E-08) to affect the field
b_2	$b_2 = -1173 + \{719*(d/D_P)\} - \{1032*(y/D_P)\} + \{763*(y/D_P)*(y/D_P)\} - \{116.2*(y/D_P)*(y/D_P)*(y/D_P)\}$
c_2	$c_2 = -99090 + \{34803*(y/D_P)\}$

Table 4.3. Regression equations for predicting K, a, b, c, a_1, b_1, c_1, a_2, b_2 and c_2 for Far Field zone

Coeff. of (A) 'K' – 'c_2'	Prediction Equations of the unknown coefficients (K ~ c_2) for **Far Field**, obtained through stepwise regression analysis incorporating up to cubic terms
K	$K = 134120 - \{6844*(x/D_P)\}$
a	$a = -0.267 + \{0.349*(d/D_P)\} + \{0.1685*(y/D_P)\} - \{0.206*(d/D_P)*(y/D_P)\}$
b	$b = 5491 - \{467*(x/D_P)*(d/D_P)\} + \{10933*(d/D_P)*(d/D_P)*(d/D_P)\}$
c	$c = -852767 + \{54310*(x/D_P)\} + \{488902*(d/D_P)\} + \{132689*(y/D_P)\} - \{902*(x/D_P)*(x/D_P)\} - \{20372*(y/D_P)*(y/D_P)\} - \{10354*(x/D_P)*(d/D_P)\} - \{194760*(d/D_P)*(y/D_P)\} + \{25978*(d/D_P)*(y/D_P)*(y/D_P)\}$
a_1	Ignored, as this coefficient is too small (average = 1.66E-03) to affect the field
b_1	$b_1 = 0.0546 - \{0.0334*(y/D_P)\} + \{0.0388*(d/D_P)*(d/D_P)*(y/D_P)\}$
c_1	$c_1 = 3713 - \{5329*(d/D_P)*(d/D_P)*(d/D_P)\}$
a_2	Ignored, as this coefficient is too small (average = - 4.76E-09) to affect the field
b_2	$b_2 = -647 + \{360*(d/D_P)\}$
c_2	$c_2 = -657734 + \{94409*(x/D_P)\} + \{78090*(y/D_P)\} - \{4593*(x/D_P)*(x/D_P)\} - \{11756*(y/D_P)*(y/D_P)\} - \{3454*(x/D_P)*(y/D_P)\} + \{71.8*(x/D_P)*(x/D_P)*(x/D_P)\} + \{570*(x/D_P)*(y/D_P)*(y/D_P)\}$

There are 10 unknown coefficients in equation (A), each of which can be derived by using the regression equations listed in Tables 4.1-4.3 for each of the three zones of interest. Stepwise regression analysis was used to model the prediction equations to determine the coefficients for up to cubic order, to maintain good prediction capacities of the equations. Hence, for a given location in

the 3D wake field, the coefficients of equation (A) can be determined, and for a given propeller condition (where n, θ, and H are known), the non-dimensionalized mean axial flow velocity can be estimated.

4 Conclusions

The present experimental investigation on a propeller wake velocity (axial) field for the major factors affecting propeller wake wash performance leads to the following concluding remarks:

- Among the three factors, propeller rotational speed is the most influential, followed by propeller inclination angle and propeller depth of submergence respectively. The propeller speed 'n' and inclination angle 'θ' affect the flow positively, whereas submergence depth 'H' affects it negatively. The effect of 'n' is always positive throughout the wake field. The effect of 'θ' is not as consistent, particularly at higher depth of measurement (such as at 1.05Dp). As 'n' increases, the effect of 'θ' also increases. As 'H' decreases, the time averaged axial velocity increases, but the risk of cavitation also increases.
- The rate of change (growth or decay) in the mean axial velocity along x/Dp in terms of 'n', 'θ', and 'H' for any depth of measurement is highest in the near field zone. For a particular configuration of factors, the velocity profile representing the distribution of axial velocities along x/Dp becomes larger with the increase of depth.
- As 'n' and 'θ' increase, the velocity distribution profile becomes larger and the effective size of the wake field increases, particularly at shallow depth of measurement. The effect of 'H' is the reverse and more inconsistent.

The above observations are for the center of the wake field (the location likely to be the most unaffected by the tank wall boundary condition), and it is expected that they will also be applicable for the entire wake field.

- The zone where the mean axial flow velocities were higher than other zones in the most of the cases is the region of $x/D_p = 7.5$ for all three 'n' (at $\theta = 4.5°$ and $H = 350$ mm) considered in the OFAT study. The location of that zone changes with 'θ', and the change is inconsistent. Furthermore, the interaction plots illustrate that the effect of 'n' is much stronger than the effect of 'θ' on the response variable in the downstream wake field, and the effect of 'θ' increases with the increase of 'n' up to a certain extent.
- A second order regression equation (as mentioned in section 3.3) can be used to predict the mean axial velocity of flow downstream of propeller wake field. The quadratic terms are also included to increase the prediction capacities of the equation. The average prediction capacity of all the equations for 168 locations is 71%. For the locations along the center of the wake field, the prediction capacity is about 84%.

The prediction equations can be used to approximate the mean axial velocity at locations within the wake field, including near the free surface. Applications of the results include predicting wake wash effects, such as those used to manage pack ice in offshore operations. The results of this investigation can also be used as a benchmark to compare with results from numerical studies.

References

1. Amin, A.: Experimental Investigation of Propeller Wake Velocity Field. Master's Thesis. Memorial University of Newfoundland, Canada. 2017.
2. Anderson, K. G.; McDonald, D.; Mitten, P.; Nicholls, S.; Tait, D.: Management of Small Ice Masses. Environmental Studies Revolving Funds, Report no. 042. 1986.
3. Bastin, T.: Mathematical Modeling of Propeller Wake Wash for Pack-ice Management. Master's Thesis. Memorial University of Newfoundland, Canada, 2014.
4. Blaauw, H. G.; Van de Kaa, E. J.: Erosion of Bottom and Sloping Banks caused by the Screw race of Maneuvering Ships. Delft Hydraulics laboratory, Netherlands, Report no. 202, 1978.
5. Berger, W.; Felkel, K.; Hager, M.; Oebius, H.; Schale, E.: Courant provoque par les bateaux protection des berges et solution pour eviter l' erosion du lit du haut rhin. In P.I.A.N.C., 25th Congress, Section I-1. Edinburgh, 1981.
6. Brewster, P. M.: Modeling the Wash from a Ship's Propeller. Ph.D Thesis. Queen's University of Belfast, UK, 1997.
7. Design Expert 10.0 Technical Support: The software manual which is used to develop the 3D surface plots and regression equations showing the relationship among factors and response.
8. Ferrieri, J. M.; Veitch, B.; Akinturk, A.: Experimental Study on Ice Management through the use of Podded Propeller Wash. Third Symposium on Marine Propulsors, Australia, 2013.
9. Fuehrer, M.; Romisch, K.: Effects of Modern Ship Traffic on Islands and Ocean Waterways and their Structures. Proceedings 24th Congress P.I.A.N.C., Leningrad, Sections1-3, 1977.
10. Hamill, G. A.: Characteristics of the Screw Wash of a Maneuvering Ship and the resulting Bed Scour. *PhD Thesis*. Queen's University of Belfast, UK, 1987.
11. Hashmi, H. N.: Erosion of a granular bed at a Quay wall by a Ship's Screw Wash. *PhD Thesis*. Queen's University of Belfast, UK, 1993.
12. Keinonen, A.J.; Lohi, P.: Azimuth and multipurpose icebreaker technology for arctic and non-arctic offshore. Proceedings, Offshore and Polar Engineering Conference, Seattle, 2000.
13. Keinonen, A. J.: Ice management for ice offshore operations. Proceedings, Offshore Technology Conference, Houston, 2008.
14. Lam, W. H.; Hamill, G. A.; Song, Y. C.: Experimental Investigation of the decay from a Ship's Propeller. China Ocean Engineering, 25:2, 265-284, 2011.
15. Lam, W.; Robinson, D. J.; Hamill, A.: Initial wash profiles from a Ship's Propeller using CFD method. Journal of Ocean Engineering, 2013.
16. McGarvey, J. A.: The influence of the Rudder on the Hydrodynamics and the resulting bed Scour of a Ship's Screw Wash. PhD Thesis. Queen's University of Belfast, UK, 1996.
17. Montgomery, D. C.: Design and Analysis of the experiments. 8th edition. John Wiley & Sons. Inc, New York, USA, 2013.
18. Stewart, D. P. J.: Characteristics of a Ship's Screw Wash and the influence of Quay Wall Proximity. PhD Thesis. Queen's University of Belfast, UK, 1992.
19. Verhey, H. J.: The Stability of Bottom Banks subjected to velocities in the Propeller Jet behind Ships. 8th International Harbor Congress, Belgium, 1983.